INSTITUTE OF PHYSICS PUBLISHING INVERSE PROBLEMS

Inverse Problems **18** (2002) 265–277 PII: S0266-5611(02)27706-0

On an integral transform and its inverse in nuclear imaging

Mai K Nguyen[1] **and T T Truong**[2]

[1]Equipe de Traitement des Images et du Signal, CNRS UPRESA 8051, ENSEA, Université de Cergy-Pontoise, Ecole Nationale Supérieure de l'Electronique et de ses Applications, 6, avenue du Ponceau, 95014 Cergy-Pontoise, France
[2]Laboratoire de Physique Théorique et Modélisation, Université de Cergy-Pontoise, 95031 Cergy-Pontoise Cedex, France

Received 8 August 2001
Published 15 January 2002
Online at stacks.iop.org/IP/18/265

Abstract

In a nuclear imaging modality, the goal is to reconstruct the object under study from photon intensity distributions on a detector. However, photon scattering, mainly as a consequence of the Compton effect, considerably affects the image quality of the object. This is why most image reconstruction methods operate only with primary or non-scattered photons. Nevertheless the restored image remains noisy and weak in intensity. In this paper a new relation between the object and photon intensity distributions, generated by photons *scattered at various deflection angles* is established. It takes the form of an integral transform, compounded from Fourier and Hankel transforms. Most importantly this new transformation is *invertible*. As a result a novel principle for image reconstruction using scattered photons is derived and may lead to the conception of a new type of imaging device.

1. Introduction

From our point of view, the working principle of a nuclear imaging system, operating either with x-rays or with gamma rays, is essentially a mapping of the object, represented by a real density function $f(\boldsymbol{r})$ with compact support in $\mathcal{R}^3$, onto measurement data, represented by a real density function $g(\boldsymbol{r}', \tau)$. Here $\boldsymbol{r}'$ denotes a measurement site on a two-dimensional detection space and τ a typical relevant parameter. Let this mapping be $\mathcal{T} : f \longrightarrow g$, or alternatively $g = \mathcal{T} f$. Then the structure of $\mathcal{T}$ is completely specified by the process of image formation in the imaging device.

Conversely, finding the object density function $f(\boldsymbol{r})$ from the image distribution $g(\boldsymbol{r}', \tau)$ (or observed images) is an image reconstruction problem. It is typically an *inverse* problem, but often an *ill-posed* one. In this case the parameter τ which brings in additional information for finding $\mathcal{T}^{-1}$ plays a crucial role in an image reconstruction procedure. As an illustration we shall review in section 2 the case of *transmission* imaging with the so-called cone beam

 © 2002 IOP Publishing Ltd Printed in the UK

projection technique where the role of τ is explicitly displayed. Our main work concerns *emission* imaging and will be presented in section 3. We describe a new transform $\mathcal{T}$ which relates the object to the distribution of scattered photons on the detector and show that $\mathcal{T}$ can be inverted. This property gives the possibility of taking advantage of scattered photons for reconstructing images, instead of eliminating them as usually done. It may open the way to a new image reconstruction method using not only primary gamma rays but also scattered ones, contributing to the improvement of signal to noise ratio (SNR) and of image quality. Conclusions and perspectives are given in section 4.

2. Integral transform in x-ray transmission imaging

X-ray transmission through media is certainly the earliest technique used in modern radiological imaging procedures and has been ever since helpful for medical diagnostics. Its working principle is based on the selective absorption properties of biological tissues by traversing x-rays, emitted from external sources. The object density function $f(\boldsymbol{r})$ is thus the medium linear absorption coefficient. The projection data density function $g(\boldsymbol{r}', \tau)$ is the relative x-ray intensity measured on a two-dimensional detector (e.g. radiographic film) which produces a radiographic picture of the organ under study (see [1], chapter 9).

However for a more accurate medical diagnostic, a three-dimensional picture of the body organ may be needed. Therefore a reconstruction of $f(\boldsymbol{r})$ must be performed. This is possible in general if a three-dimensional collection of projection data density $g(\boldsymbol{r}', \tau)$ is available and provides the necessary information for the inversion of $\mathcal{T}$. In this section, we discuss the technique of cone beam projection to illustrate their connection with integral transforms and their inverses.

The object, in this case is illuminated by a conical beam of x-rays coming from a point source at a site $\boldsymbol{r}''(\tau)$, located on a space curve *parametrized* by τ [2]. At a site $\boldsymbol{r}'$ on the detector the measured data $g(\boldsymbol{r}', \tau)$ is the line integral (from $\boldsymbol{r}''$ to $\boldsymbol{r}'$) of the object density function $f(\boldsymbol{r})$, which is the logarithm of the normalized intensity of the x-ray beam traversing the object:

$$g(\boldsymbol{r}', \tau) = \int_0^1 \mathrm{d}s \; f(\boldsymbol{r}''(\tau) + (\boldsymbol{r}' - \boldsymbol{r}''(\tau))s). \tag{1}$$

For a given point source position $\boldsymbol{r}''$, measurements should be made at all detector sites $\boldsymbol{r}'$, so as to catch all relevant x-rays passing through the object.

The problem is now to compute $f(\boldsymbol{r})$ from the measured $g(\boldsymbol{r}', \tau)$. To do this, one uses the Radon transform, which associates to each function $h(\boldsymbol{r})$, its integral on a plane with normal unit vector $\boldsymbol{n}$ and at a distance ρ from the origin of coordinates:

$$\mathcal{R}h(\rho, \boldsymbol{n}) = \int \mathrm{d}\boldsymbol{r} \; \delta(\boldsymbol{r} \cdot \boldsymbol{n} - \rho) h(\boldsymbol{r}). \tag{2}$$

The Radon transform is invertible and its inversion yields the formula [7, 11]:

$$h(\boldsymbol{r}) = -\frac{1}{8\pi^2} \int \mathrm{d}\boldsymbol{n} \, \frac{\partial^2}{\partial \rho^2} \mathcal{R}h(\rho, \boldsymbol{n})|_{\rho = \boldsymbol{r} \cdot \boldsymbol{n}}, \tag{3}$$

this is an integral over all space directions of $\boldsymbol{n}$ of a radial second derivative of $\mathcal{R}h(\rho, \boldsymbol{n})$. However, the measured data $g(\boldsymbol{r}', \tau)$ does not appear as Radon data. The conversion from measured data to Radon data is not a trivial task. To see this difficulty, let us consider the restriction of the object density function $f(\boldsymbol{r})$ on a plane (P) containing the point source $\boldsymbol{r}''(\tau)$ and orthogonal to the planar detector: $f_{\rho,n}(r, \phi)$, where (r, ϕ) are the polar coordinates

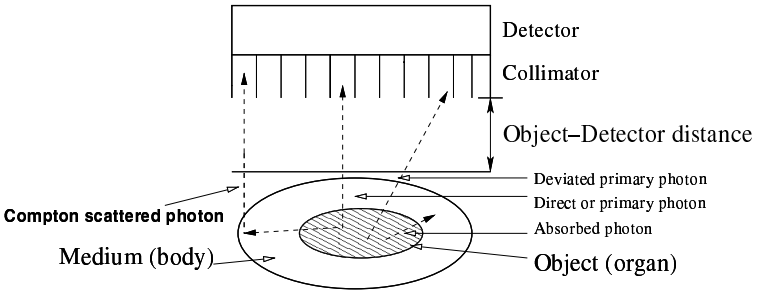

Figure 1. Principle of emission imaging with a gamma camera.

of a running point in (P). Then the Radon transform of $f(\boldsymbol{r})$ along (P) is simply the surface integral

$$\mathcal{R}f(\rho, \boldsymbol{n}) = \iint r \, \mathrm{d}\phi \, \mathrm{d}r \; f_{\rho,\boldsymbol{n}}(r, \phi). \tag{4}$$

But the measured quantity is the line integral: $\int f_{\rho,\boldsymbol{n}}(r, \phi) \, \mathrm{d}r$. The problem of converting measured data into Radon data was solved by Grangeat [3] and generalized by Tam [4]. These authors have established a relation between $\frac{\partial}{\partial \rho}\mathcal{R}f(\rho, \boldsymbol{n})$ and $g(\boldsymbol{r}', \tau)$, such that with measured data multiplied by an appropriate weighting function, for all possible ray directions and all possible source positions $\boldsymbol{r}''(\tau)$, the inverse can be calculated. In fact, the derivative of the line integrals along a direction perpendicular to the integration direction are identical to the radial derivative of the Radon data. Inserting this result back to the inversion formula of the Radon transform, one can obtain the reconstruction of $f(\boldsymbol{r})$. Here the transformation $\mathcal{T}$ is of course the Radon transform.

However it is essential to find out under what conditions a space curve as trajectory of the x-ray point source $\boldsymbol{r}(\tau)$ would yield a complete set of projection data. The solution to this question is obtained by Tuy [5], who gave a sufficient condition on admissible space curves parametrized by τ. Then after gathering data for all relevant τ, one may obtain the three-dimensional inversion of the transformation $\mathcal{T}$.

3. Emission imaging with Compton scattered photons

3.1. Set-up and working principle

In nuclear medicine the images are formed using the gamma rays emitted from a radionuclide absorbed and unevenly distributed in the patient's body. In particular, for example, there will be strong accumulation of the radiopharmaceutical in a malignant region, rendering it visible on a gamma-ray camera. Basically this apparatus consists of three superimposed parts, as shown in figure 1:

- a collimator with parallel holes drilled in a block of lead to select only incoming photons travelling perpendicularly to the detector plane,
- a crystal scintillator for converting photon energy into light,
- a set of photomultipliers and electronic devices to amplify signals or photon counts and to store measured data.

Ideally only photons travelling along the axis of the collimator will reach the detector and there are four signals for recording:

- the number of photons at a site per unit time,
- the two coordinates of the arrival site,
- the energy of each incoming photon.

In the normal 'frame' mode, only photons, called primary photons belonging to the sharply defined emission energy of the radionuclide (e.g. $E_0 \sim 140\,\mathrm{keV}$ for ^{99m}Tc sources) and entering the collimator along its axis are collected. But they represent only a very small part (around one in 10^4 photons) of the total number of emitted photons. The recorded image is thus weak in intensity and also suffers from additional causes of degradation such as attenuation due to absorption by the traversed medium and overwhelmingly Compton scattering by free electrons in the surrounding medium. Up to now, most efforts are devoted to the restoration of the image in such gamma cameras, by elimination of the scattered photons.

3.2. Compton scattering

So perhaps it is meaningful to look at those of the emitted photons which undergo Compton scattering at various levels and study how they may turn out to be relevant for image improvement [6]. Before dealing with the heart of the matter we shall first recall some facts about Compton scattering (see [1], vol 1, appendix C.3).

At sufficiently high energy photons exhibit particle behaviour and are elastically scattered by free electrons at rest in the biological medium of the body. A scattered photon goes off with an energy

$$E = E_0 \frac{1}{1 + \varepsilon(1 - \cos\theta)} \tag{5}$$

where θ is the scattering angle as measured from the incident photon direction; E_0, the photon initial energy; ε, the ratio $\frac{E_0}{mc^2}$ and mc^2 the rest energy of the electron. The Compton scattering is also a quantum phenomena: the emergence of the scattered photon has a probability of occurrence given by the Compton differential cross section

$$\frac{\mathrm{d}\sigma}{\mathrm{d}\Omega} = \frac{r_e^2}{2} P(\theta) \tag{6}$$

where r_e is the classical radius of the electron and $P(\theta)$ the so-called Klein–Nishina probability for deflection by an angle θ:

$$P(\theta) = \frac{1}{[1 + \varepsilon(1 - \cos\theta)]^2} \left[1 + \cos^2\theta + \frac{\varepsilon^2 (1 - \cos\theta)^2}{1 + \varepsilon(1 - \cos\theta)} \right]. \tag{7}$$

As a result of Compton scattering, photons leaving an emitting point source can enter the collimator along the direction of its axis after one or more scattering. However, since measurements and Monte Carlo simulations [13] show that single-scattered photons dominate the process, we shall limit ourselves to single-scattered photons.

Equation (5) shows that single-scattered photons have a continuous energy spectrum: $0 \leqslant E \leqslant E_0$ related to the scattering angle θ. Thus at given angle θ, let $g(\boldsymbol{r}', \theta)$ be the photon intensity density per unit time at detector site $\boldsymbol{r}'$ (of course here $\tau = \theta$). This quantity describes essentially a *secondary* emission imaging process since it is based on secondary emission sites (collision sites) formed by the free electrons of the body biological medium. In a conventional γ-ray image processing, they are discarded by filtering or by other techniques. The question at hand is whether or not such *secondary* images so obtained are of any interest.

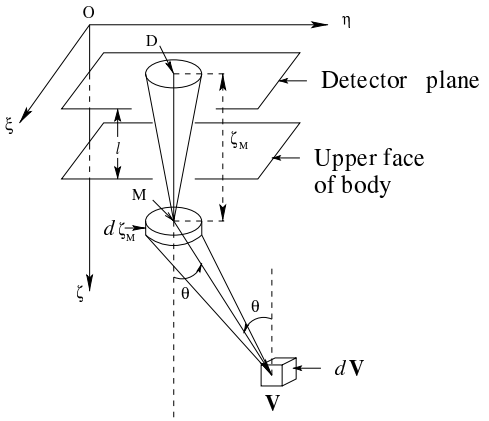

Figure 2. Flux of photons arriving at the detector plane.

3.3. Integral transform $\mathcal{T}$ related to secondary emission imaging

Again let $f(\boldsymbol{r})$ be the object density function of the organ under consideration. As in gamma imaging an emission site $\boldsymbol{r}$ is called a voxel [1], we shall adopt the notation $\boldsymbol{r} = \boldsymbol{V}$, so that $f(\boldsymbol{r}) = f(\boldsymbol{V}) = f(\xi_V, \eta_V, \zeta_V)$. This is also the number of photons emitted per unit time and per unit object (or source) volume, uniformly distributed around the 4π solid angle at site $\boldsymbol{V}$, see figure 2.

Consequently in one given direction, making an angle θ with the vertical downward direction $O\zeta$, the number of photons emitted in a small solid angle $\mathrm{d}\Omega_M$ around site M by an elemental source volume $\mathrm{d}\boldsymbol{V}$, per unit time is

$$\frac{1}{4\pi} f(\boldsymbol{V})\,\mathrm{d}\boldsymbol{V}\,\mathrm{d}\Omega_M. \tag{8}$$

Now we have $\mathrm{d}\Omega_M = \frac{\mathrm{d}\sigma_M}{MV^2}$, where $\mathrm{d}\sigma_M$ is the area element around site $\boldsymbol{M}$ normal to the direction VM (see figure 2). Consequently the flux of photons arriving at $\boldsymbol{M}$ in the VM direction is

$$\frac{f(\boldsymbol{V})\,\mathrm{d}\boldsymbol{V}}{4\pi}\,\frac{1}{MV^2}. \tag{9}$$

To focus on the Compton effect, we have neglected photon absorption by body tissues, which is a separate physical phenomena.

But at site $\boldsymbol{M}$, there are $n_e\,\mathrm{d}\boldsymbol{M}$ free electrons in a small volume element $\mathrm{d}\boldsymbol{M}$, where n_e is the electron density assumed to be constant in body tissues. Now since $\left(\frac{\mathrm{d}\sigma}{\mathrm{d}\Omega}\right)\mathrm{d}\Omega_D$ is the differential cross section of photons scattering in the θ-direction, and since $\mathrm{d}\Omega_D = \frac{\mathrm{d}\sigma_D}{DM^2}$, the number of photons reaching a unit detector surface at $\boldsymbol{D}$ per unit time (after division by the area $\mathrm{d}\sigma_D$) is

$$\frac{f(\boldsymbol{V})\,\mathrm{d}\boldsymbol{V}}{4\pi}\,\frac{1}{MV^2}\,n_e\,\mathrm{d}\boldsymbol{M}\,\frac{r_e^2}{2}\,P(\theta)\,\frac{1}{MD^2}. \tag{10}$$

Consequently the number of photons recorded per unit time and unit detector area at site $\boldsymbol{D}$ of coordinates (ξ_D, η_D) due to all emitting point sources $\boldsymbol{V}$ with one scattering on the vertical line MD at site $\boldsymbol{M}$ at angle θ is given by the integral

$$g(\boldsymbol{D},\theta) = \int \mathrm{d}\xi_M\,\mathrm{d}\eta_M\,n_e\delta(\xi_D-\xi_M)\delta(\eta_D-\eta_M)\int \frac{\mathrm{d}\zeta_M}{\zeta_M^2}\,\frac{f(\boldsymbol{V})\,\mathrm{d}\boldsymbol{V}}{4\pi}\,\frac{\delta(\mathrm{Cone})}{MV^2}\,\frac{r_e^2}{2}P(\theta), \tag{11}$$

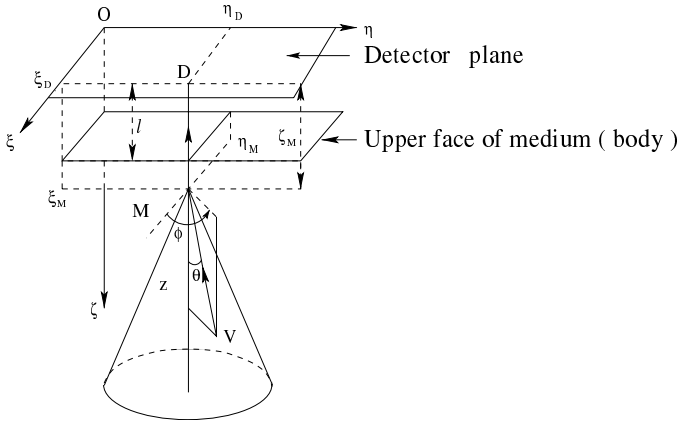

Figure 3. Coordinate system for the calculation of $\mathcal{T}$.

where δ(Cone) restricts the integration over $\boldsymbol{V}$ to the circular cone of axis parallel to $O\zeta$, of apex $\boldsymbol{M}$ and opening angle θ. Clearly $g(\boldsymbol{D}, \theta)$ has the dimension of a photon flux density through a plane. Thus we have the mapping

$$\mathcal{T} : f(\boldsymbol{V}) \longmapsto g(\boldsymbol{D}, \theta). \tag{12}$$

Note that $g(\boldsymbol{D}, \theta)$ is a function belonging to a space of sufficiently smooth functions with compact support in $\mathcal{R}^2$ and depending on a parameter θ, whereas $f(\boldsymbol{V})$ can be a distribution with compact support in $\mathcal{R}^3$.

3.4. Explicit expression of $\mathcal{T}$

In the coordinate system presented in figure 3, the measuring apparatus formed by the collimator, the detector and the photomultiplier bank is collapsed into a rectangle in the horizontal plane $O\xi\eta$. The positive vertical axis $O\zeta$ is, as already seen, directed downward. The upper side of the patient body is schematically limited by a horizontal plane of equation $\xi = l$, and we assume that the patient's body lies in the space below this plane and that $f(\boldsymbol{V})$ has compact support.

Moreover we consider a range of scattered energies such that the scattering angle θ sweeps the interval $0 < \theta < \pi$. It turns out that this range provides complete information for the reconstruction of the object. But sometimes in radiological imaging, parameters do not have to sweep the entire geometrical range (see in [1], vol 2 section 9.3.2). The coordinates of $\boldsymbol{V}$ in this system are

$$\xi_V = \xi_M + r\sin\theta\cos\phi, \qquad \eta_V = \eta_M + r\sin\theta\sin\phi, \qquad \zeta_V = \zeta_M + r\cos\theta,$$

where $VM = r$, θ is the scattering angle and ϕ the azimuthal angle of $\boldsymbol{V}$ with respect to the cone axis DM. The integration measure on the cone is $r\sin\theta\,\mathrm{d}\phi\,\mathrm{d}r$. Hence equation (11) after integration over ξ_M and η_M becomes

$$g(\boldsymbol{D}, \theta) = K(\theta)\int_l^\infty \frac{\mathrm{d}\zeta_M}{\zeta_M^2}\int_0^{2\pi}\mathrm{d}\phi \times \int_0^\infty \frac{\mathrm{d}r}{r} f(\xi_D + r\sin\theta\cos\phi, \eta_D + r\sin\theta\sin\phi, \zeta_M + r\cos\theta) \tag{13}$$

where the factor $K(\theta)$ contains the terms dependent on θ

$$K(\theta) = \frac{n_e}{4\pi}\frac{r_e^2}{2}P(\theta)\sin\theta. \tag{14}$$

In the expression (13) of $g(\boldsymbol{D},\theta)$, the integral on r is formally divergent near the origin since $f(\boldsymbol{V})$ is a bounded function (the activity density is everywhere finite). When $r \longrightarrow 0$ it means that $\boldsymbol{V} \longrightarrow \boldsymbol{M}$. Physically the primary point source $\boldsymbol{V}$ is sitting on top of the secondary point source $\boldsymbol{M}$. In this case it is the primary photon emission (of energy E_0) which takes over, and the secondary process is left out. Moreover electrons and photon emitting nuclei, being quantum mechanical particles cannot be point-wise localized. So their separation can be at best limited by the smallest of their Compton wavelengths: ϵ. Mathematically, the regularization of the integral in equation (13) can be achieved by assigning ϵ as a cut-off for the integration in r. We write thus

$$g(\boldsymbol{D},\theta) = \lim_{\epsilon\to 0} K(\theta)\int_l^\infty \frac{\mathrm{d}\zeta_M}{\zeta_M^2}\int_0^{2\pi}\mathrm{d}\phi \times \int_\epsilon^\infty \frac{\mathrm{d}r}{r} f(\xi_D + r\sin\theta\cos\phi,\, \eta_D + r\sin\theta\sin\phi,\, \zeta_M + r\cos\theta). \tag{15}$$

As $f(\boldsymbol{V})$ is of compact support, this integral can be understood as the sum of integrals of $f(\boldsymbol{V})$ on cones of axis parallel to $O\zeta$, apex $\boldsymbol{M}$ and opening angle $\theta \in]0,\pi[$ combined with sums over different altitudes of $\boldsymbol{M}$. The object is thus represented by a set of *conical integrals* instead of planar integrals. In this sense one may view this transformation $\mathcal{T}$ as a *generalized* Radon transform.

Note that the conical integral part has been introduced earlier in a simpler context [8], in which the apex of the cones are confined in a plane, instead of being in the entire biological medium volume.

The point is now to determine whether or not this transformation is *invertible* and lends itself to the process of object reconstruction.

3.5. The $\mathcal{T}$-transform as a compound Fourier–Hankel transform

To this end, a more transparent form of $\mathcal{T}$ is obtained by performing some transformations on equation (15). First we introduce the two-dimensional Fourier transform of $f(\boldsymbol{V})$ under the form

$$F(u,v,\zeta_M) = \iint \mathrm{d}\xi_D\,\mathrm{d}\eta_D\, f(\xi_D,\eta_D,\zeta_M;\theta)\exp[-2\mathrm{i}\pi(u\xi_D + v\eta_D)], \tag{16}$$

and a similar transform $\tilde{G}(u,v,\theta)$ for $g(\boldsymbol{D},\theta)$. So by applying the Fourier transform to equation (15), we get an alternative form:

$$\tilde{G}(u,v,\theta) = \lim_{\epsilon\to 0} K(\theta)\int_l^\infty \frac{\mathrm{d}\zeta_M}{\zeta_M^2}\int_\epsilon^\infty \frac{\mathrm{d}r}{r}F(u,v,\zeta_M + r\cos\theta) \times \int_0^{2\pi}\mathrm{d}\phi\,\exp[2\mathrm{i}\pi r\sin\theta\,(u\cos\phi + v\sin\phi)]. \tag{17}$$

Now setting $u = \sqrt{u^2+v^2}\cos\psi$ and $v = \sqrt{u^2+v^2}\sin\psi$, we may perform the angular integration and get the Bessel function $J_0(x)$ [9], so that

$$\tilde{G}(u,v,\theta) = \lim_{\epsilon\to 0} 2\pi K(\theta)\int_l^\infty \frac{\mathrm{d}\zeta_M}{\zeta_M^2} \times \int_\epsilon^\infty \frac{\mathrm{d}r}{r}F(u,v,\zeta_M + r\cos\theta)J_0\left(2\pi\sqrt{u^2+v^2}r\sin\theta\right). \tag{18}$$

For a better insight and understanding of the nature of $\mathcal{T}$, we define the function

$$H(u, v, r\cos\theta) = \int_l^\infty \frac{\mathrm{d}\zeta_M}{\zeta_M^2} F(u, v, \zeta_M + r\cos\theta) \tag{19}$$

and introduce the change of variables $z = r\cos\theta$ and $t = \tan\theta$. Note that for $0 < \theta \leqslant \frac{\pi}{2}$, both z and t are positive. With the dependence on θ replaced by the dependence on t, $\tilde{G}(u, v, \theta)$ becomes $G(u, v, t)$ and equation (18) now appears as

$$\frac{G(u, v, t)}{K(t)} = \lim_{\epsilon' \to 0} 2\pi \int_{\epsilon'}^\infty z\,\mathrm{d}z\, J_0\left(2\pi z\sqrt{u^2 + v^2}t\right) \frac{H(u, v; z)}{z^2}$$

with $\epsilon' = \epsilon\cos\theta$.

However, a proper way around the divergence problem is to calculate the derivative of the previous equation with respect to t. Since $J_0' = -J_1$ [9], we have

$$\frac{\partial}{\partial t}\frac{G(u, v; t)}{K(t)} = \lim_{\epsilon' \to 0} (-4\pi^2)\sqrt{u^2 + v^2} \int_{\epsilon'}^\infty z\,\mathrm{d}z\, J_1\left(2\pi z\sqrt{u^2 + v^2}t\right) \frac{H(u, v; z)}{z}. \tag{20}$$

The right-hand side of equation (20) is clearly finite for $\epsilon' \to 0$, so that from now on we need not write the limiting procedure. This shows precisely that

$$\frac{(-1)}{2\pi\sqrt{u^2 + v^2}} \frac{\partial}{\partial t}\frac{G(u, v; t)}{K(t)}$$

is the first-order Hankel transform [10, 11] of the function $H(u, v; z)z^{-1}$.

3.6. Inversion of $\mathcal{T}$

In this section we show that for $0 < \theta < \pi$ it is possible to express $f(\boldsymbol{V})$ in terms of the measured data $g(\boldsymbol{D}, \theta)$. Data taken in this range of θ yield complete information for the reconstruction of the object density function.

Now in the range $0 < \theta \leqslant \frac{\pi}{2}$, equation (20) shows that the pair of variables conjugate in the first-order Hankel transform is $z \leftrightarrow \left(t\sqrt{u^2 + v^2}\right)$. But as it is known, the Hankel transform is self-similar and invertible as the Fourier transform is [10]. Recalling the definition of $H(u, v; z)$, we can thus invert the Hankel transform:

$$\frac{1}{z}\int_l^\infty \frac{\mathrm{d}\zeta_M}{\zeta_M^2} F(u, v, \zeta_M + z) = -2\pi\sqrt{u^2 + v^2} \int_0^\infty t\,\mathrm{d}t\, J_1\left(2\pi z\sqrt{u^2 + v^2}t\right) \frac{\partial}{\partial t}\frac{G(u, v; t)}{K(t)}. \tag{21}$$

We make now a change of variables $s = (\zeta_M - l)$ and $\sigma = (z + l)$ to reexpress $H(u, v; z)$ (on the left-hand side of the last equation (21)), as

$$\int_l^\infty \frac{\mathrm{d}\zeta_M}{\zeta_M^2} F(u, v, \zeta_M + z) = \int_0^\infty \frac{\mathrm{d}s}{(s + l)^2} F(u, v, s + \sigma). \tag{22}$$

Going to the Fourier representation of $F(u, v, s + \sigma)$ in the third variable

$$F(u, v, s + \sigma) = \int_{-\infty}^\infty \mathrm{d}w\, \bar{F}(u, v, w) \exp[-2\mathrm{i}\pi w(s + \sigma)], \tag{23}$$

where $\bar{F}(u, v, w)$ is actually the three-dimensional Fourier transform of $F(\boldsymbol{V})$, since from equation (16) we see that u and v are already the Fourier variables of the two first coordinates ξ_D and η_D of $f(\boldsymbol{V})$. Recalling that $z = r\cos\theta$ we have

$$H(u, v, z) = \int_{-\infty}^\infty \mathrm{d}w\, \bar{F}(u, v, w) \exp(-2\mathrm{i}\pi w\sigma) \int_0^\infty \frac{\mathrm{d}s}{(s + l)^2} \exp(-2\mathrm{i}\pi ws). \tag{24}$$

The last integral of the previous equation is nothing but the Fourier transform of the generalized function $Y(s)(s+l)^{-2}$, $Y(s)$ being the unit-step Heaviside function. Its value is given in Fourier tables [12] (e.g. Lavoine's table, p 88):

$$\int_0^\infty \frac{\mathrm{d}s}{(s+l)^2} \exp(-2\mathrm{i}\pi ws) = \mathcal{J}_l(w) \tag{25}$$

with

$$\mathcal{J}_l(w) = 2\mathrm{i}\pi w \left\{ \exp 2\mathrm{i}\pi lw\big[\mathrm{Ci}(2\pi l|w|) - \mathrm{i}\,\mathrm{Sgn}(w)\,\mathrm{Si}(2\pi l|w|)\big] - \frac{\mathrm{i}}{2\pi wl} \right\},$$

where $\mathrm{Sgn}(w)$ is the sign function of w, $\mathrm{Ci}(w)$ and $\mathrm{Si}(w)$ are the cosine and sine integral functions of w (for their definitions see [9]).

Combining the results of equations (24), (25) and putting them back in the above equation (21), we get

$$\int_{-\infty}^{\infty} \mathrm{d}w\, \bar{F}(u,v,w)\mathcal{J}_l(w)\exp(-2\mathrm{i}\pi w\sigma)$$
$$= -2\pi(\sigma - l)\sqrt{u^2+v^2} \int_0^\infty t\,\mathrm{d}t\, J_1\left(2\pi t(\sigma-l)\sqrt{u^2+v^2}\right) \frac{1}{2\pi}\frac{\partial}{\partial t}\frac{G(u,v,t)}{K(t)}. \tag{26}$$

Recalling that the variable $\sigma = (z+l)$ is positive, we see that σ cannot yet be used as a variable to perform the inverse Fourier transform to extract $\bar{F}(u,v,w)$, from which the object density $f(\boldsymbol{V})$ can be reconstructed:

$$f(\boldsymbol{V}) = \int_{-\infty}^{\infty}\int_{-\infty}^{\infty}\int_{-\infty}^{\infty} \mathrm{d}u\,\mathrm{d}v\,\mathrm{d}w\, \bar{F}(u,v,w)\exp[2\mathrm{i}\pi(u\xi_V + v\eta_V + w\zeta_V)]. \tag{27}$$

To do so, one needs an extension of equation (26) for negative values of σ. Observe that both $G(u,v,t)$ and its derivative with respect to t are involved in the object reconstruction and that $K(t)$ is given by equation (14). The parameter l may be chosen arbitrarily small.

Now in the range $\theta \in]\frac{\pi}{2}, \pi[$, both z and t are negative, i.e. $(z,t) \in]-\infty, 0[$. We may set $z = -z'$ and $t = -t'$ where both z' and t' are positive and instead of equation (20) we have

$$\frac{\partial}{\partial t}\frac{G(u,v,-t')}{K(-t')} = (-4\pi^2)\sqrt{u^2+v^2}\int_0^\infty dz'\, J_1\left(2\pi z't'\sqrt{u^2+v^2}\right)\int_0^\infty \frac{\mathrm{d}\zeta}{\zeta^2} F(u,v,\zeta - z').$$

The inversion procedure goes through again except that one must take care of the change in sign for z. Equation (26) appears now, after renaming of some integration variables under the form

$$\int_{-\infty}^{\infty} \mathrm{d}w\, \bar{F}(u,v,w)\mathcal{J}_l(w)\exp(-2\mathrm{i}\pi w(l-z))$$
$$= -z\sqrt{u^2+v^2}\int_0^\infty t\,\mathrm{d}t\, J_1\left(2\pi zt\sqrt{u^2+v^2}\right)\frac{\partial}{\partial t}\frac{G(u,v,-t)}{K(-t)}.$$

Finally combining the two forms of equation (26) we have

$$\int_{-\infty}^{\infty} \mathrm{d}w\, \mathcal{J}_l(w)\,\bar{F}(u,v,w)\exp(-2\mathrm{i}\pi w(l+z)) = -|z|\sqrt{u^2+v^2}$$
$$\times \int_0^\infty t\,\mathrm{d}t\, J_1\left(2\pi|z|t\sqrt{u^2+v^2}\right)$$
$$\times \left\{ Y(z)\frac{\partial}{\partial t}\frac{G(u,v,t)}{K(t)} + Y(-z)\frac{\partial}{\partial t}\frac{G(u,v,-t)}{K(-t)} \right\}.$$

So, recalling that $\sigma = (z + l)$, $\bar{F}(u, v, w)$ can be extracted as follows:

$$\bar{F}(u, v, w) = \int \mathrm{d}\sigma \exp[2\mathrm{i}\pi\sigma w] \frac{\left[-|z|\sqrt{u^2 + v^2}\right]}{\mathcal{J}_l(w)} \int_0^\infty t\,\mathrm{d}t\, J_1\left(2\pi|z|t\sqrt{u^2 + v^2}\right) \times \left\{ Y(z)\frac{\partial}{\partial t}\frac{G(u, v, t)}{K(t)} + Y(-z)\frac{\partial}{\partial t}\frac{G(u, v, -t)}{K(-t)} \right\}. \tag{28}$$

The object density function $f(\boldsymbol{V})$ is, in turns reconstructed by Fourier transform, as indicated in equation (27).

For the special value $\theta = \frac{\pi}{2}$, the cone collapses into a plane parallel to $O\xi\eta$. The cone integral becomes now a planar integral or a Radon transform associated to planes parallel to the detector.

In the two next subsections we shall consider two special situations, where calculations can be analytically performed: plane wave approximation and point source.

3.7. Plane wave approximation and transformation $\mathcal{T}^*$

An interesting situation arises if the distance l is large compared to the size of the object. Then one may assume that re-emitted photons propagate as a beam of parallel rays (plane waves). The number of photons reaching a unit detector surface at $\boldsymbol{D}$ per unit time is the expression given by equation (9) multiplied by the Klein–Nishina probability $P(\theta)$:

$$\frac{f(\boldsymbol{V})\,\mathrm{d}\boldsymbol{V}}{4\pi}\frac{1}{MV^2}\,n_e\,\mathrm{d}\boldsymbol{M}\,P(\theta).$$

The function $H(u, v, z)$ is now

$$H = H^*(u, v, z) = \int_l^\infty \mathrm{d}\zeta_M\, F(u, v, \zeta_M + z). \tag{29}$$

Under the same change of variables as in equation (22), and using again the Fourier representation of equation (23) [12], we obtain the expression

$$H^*(u, v, z) = \int_\infty^\infty \mathrm{d}w\, \bar{F}(u, v, w) \exp(-2\mathrm{i}\pi w(z + l)) \frac{1}{2}\left[\delta(w) + Pf\frac{1}{\mathrm{i}\pi w}\right]. \tag{30}$$

This brings up a relation giving $\bar{F}(u, v, w)$ in terms of $G(u, v, t)/K^*(t)$ via equation (20) after integration over w:

$$\bar{F}(u, v, 0) + \int_{-\infty}^\infty \mathrm{d}w\, \bar{F}(u, v, w) Pf \frac{\exp(2\mathrm{i}\pi(z + l)w)}{\mathrm{i}\pi w} = 2\pi z^2(u^2 + v^2) \int_0^\infty t\,\mathrm{d}t\, J_0\left(2\pi tz\sqrt{u^2 + v^2}\right) \frac{G(u, v, t)}{K^*(t)} \tag{31}$$

with $K(t) = \frac{1}{2}r_e^2 K^*(t)$.

Now by derivation with respect to z and by Fourier transformation we obtain directly the two-dimensional Fourier transform of the object density function (which describes the sought activity density function):

$$-F(u, v, z + l) = 4\pi z(u^2 + v^2) \int_0^\infty t\,\mathrm{d}t \left[J_0\left(2\pi tz\sqrt{u^2 + v^2}\right) - z\pi\sqrt{u^2 + v^2} J_1\left(2\pi tz\sqrt{u^2 + v^2}\right)\right] G(u, v, t)\frac{1}{K^*(t)} \tag{32}$$

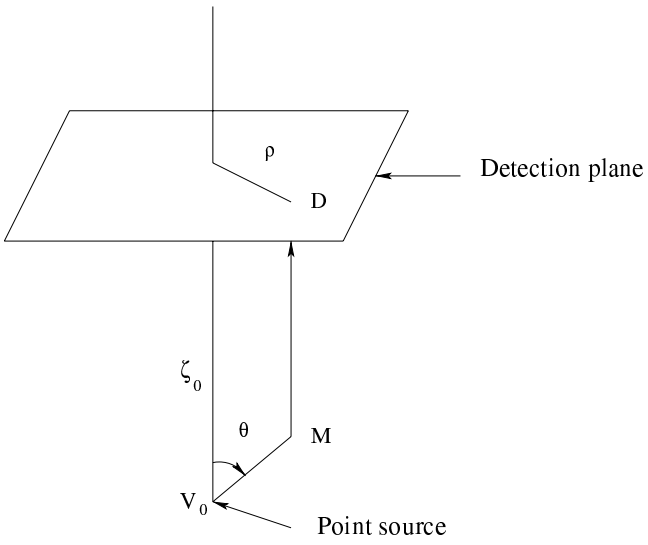

Figure 4. Coordinates for the calculation of the PSF.

since the derivative of the Bessel function J_0 is $-J_1$. Finally $f(\boldsymbol{V})$ is recovered explicitly by two-dimensional Fourier transformation, after setting $\zeta_V = z + l$:

$$f(\boldsymbol{V}) = \int_{-\infty}^{\infty}\int_{-\infty}^{\infty} \mathrm{d}u\,\mathrm{d}v\,\exp[-2\mathrm{i}\pi(u\xi_V + v\eta_V)]\,4\pi(\zeta_V - l)(u^2+v^2)$$
$$\times \int_0^{\infty} t\,\mathrm{d}t\,G(u,v,t)\frac{1}{K^*(t)}\left[-J_0\left(2\pi t(\zeta_V - l)\sqrt{u^2+v^2}\right)\right.$$
$$\left. -(\zeta_V - l)\,\pi\sqrt{u^2+v^2}\,J_1\left(2\pi t(\zeta_D - l)\sqrt{u^2+v^2}\right)\right]. \tag{33}$$

The inversion of the transformation $\mathcal{T}^*$ is thus fully performed with more tractable functions. Note that, as z is positive, ζ_V is larger than l.

3.8. Image of a point source or point spread function (PSF)

As a second special case, let us consider a point-like object located at $\boldsymbol{V}_0$ of coordinates (ξ_0, η_0, ζ_0), see figure 4, given by

$$f(\boldsymbol{V}) = f_0\delta(\xi_V - \xi_0)\delta(\eta_V - \eta_0)\delta(\zeta_V - \zeta_0), \tag{34}$$

then from the general expression (see equation (11)) after integration on $\boldsymbol{V}$, the image density function is

$$g(\boldsymbol{D},\theta) = \frac{1}{8\pi}\int \mathrm{d}\xi_M\,\mathrm{d}\eta_M\,\delta(\xi_D - \xi_M)\delta(\eta_D - \eta_M)n_e\int\frac{\mathrm{d}\zeta_M}{\zeta_M^2}f_0\delta(\mathrm{Cone})\frac{1}{M\,V_0^2}r_e^2\,P(\theta). \tag{35}$$

Now the $\delta(\xi_D - \xi_M)\delta(\eta_D - \eta_M)$ function means that $\boldsymbol{M}$ is on the vertical line perpendicular to the detector at site $\boldsymbol{D}$. Hence after the $\mathrm{d}\xi_M\,\mathrm{d}\eta_M$ integration, it remains to take care of $\delta(\mathrm{Cone})$, which dictates that $\boldsymbol{M}$ must be placed such that the angle between $M\,V_0$ and $M\,D$ is θ as specified by the scattering condition at energy E, see equation (5). Consequently, we call $g(\boldsymbol{D},\theta) = h(\boldsymbol{D},\boldsymbol{V};\theta)$ the point spread function (PSF) of this transformation, and give its expression:

$$h(\boldsymbol{D},\boldsymbol{V};\theta) = f_0\frac{n_e}{4\pi}\frac{r_e^2}{2}P(\theta)\sin\theta\,\frac{t^2}{\rho^2}\frac{Y((\zeta_0 - l)t - \rho)}{(\zeta_0 t - \rho)^2}$$

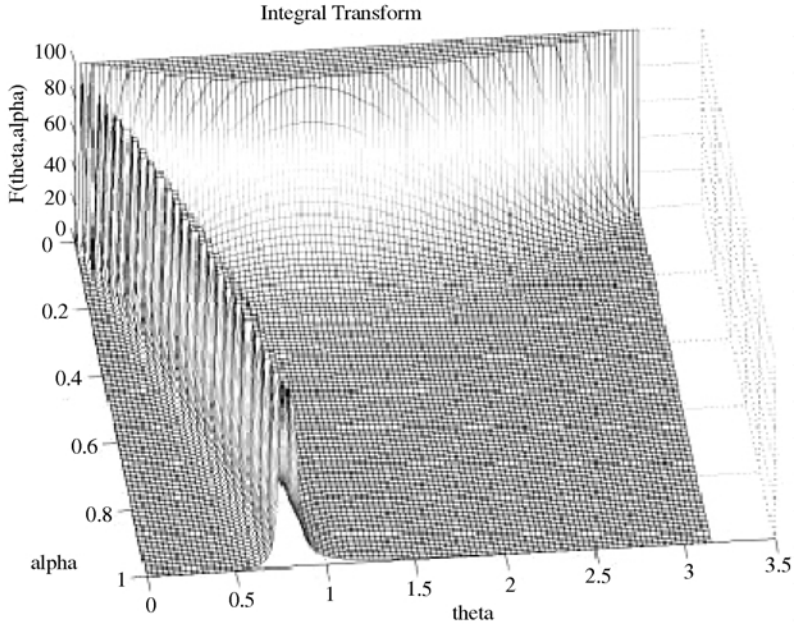

Figure 5. Behaviour of the PSF as a function of θ and the ratio $\alpha = \rho/\zeta_0$.

where $\rho = \sqrt{(\xi_0 - \xi_D)^2 + (\eta_0 - \eta_D)^2}$, and $\zeta_M = (\zeta_0 - \rho \cot\theta)$, see figure 4.

Thus one has after replacing t by $\tan\theta$

$$h(\boldsymbol{D}, \boldsymbol{V}; \theta) = f_0 \frac{n_e}{4\pi} \frac{r_e^2}{2} P(\theta) \sin\theta^3 \frac{1}{(\zeta_0 \rho)^2} \frac{Y((\zeta_0 - l)\tan\theta - \rho)}{(\sin\theta - \frac{\rho}{\zeta^0})^2}. \tag{36}$$

So this function depends on ρ, the altitude of the point-like source ζ_0 and the scattering angle θ. The image is rotationally symmetric with respect to the projection of $\boldsymbol{V}$ in the detector plane. In figure 5 we have given the behaviour of the PSF as function of θ and ρ, by plotting the expression $F(\theta, \alpha)$, as function of θ and $\alpha = \rho/\zeta_0$

$$F(\theta, \alpha) = \alpha^{-2} \frac{\sin^3\theta \; P(\theta)}{(\sin\theta - \alpha\cos\theta)^2}. \tag{37}$$

The curves at constant α are reminiscent of curves obtained by Monte Carlo simulations [13].

Now from three measured values of $h(\boldsymbol{D}_j, \boldsymbol{V}; \theta_j)$ with $j = 1, 2, 3$, one can use expression (36) to calculate the coordinates of the point source $\boldsymbol{V}$, by solving a system of three equations with three unknowns (ξ_V, η_V, ζ_V). This inverse problem, in principle, can be recast in a geometrical setting as a problem of intersection of three cones. It will be discussed elsewhere.

If one chooses this PSF with unit intensity, i.e. $f_0 = 1$, the image density function $g(\boldsymbol{D}, \theta)$ may be expressed in terms of $h(\boldsymbol{D}, \boldsymbol{V}; \theta)$ as

$$g(\boldsymbol{D}, \theta) \simeq K(\theta) \sin^3\theta \int \mathrm{d}\boldsymbol{V} \, f(\boldsymbol{V}) \frac{1}{\rho^2 (\zeta_V \sin\theta - \rho\cos\theta)^2}.$$

Again care must be exercised when dealing with the divergence in the integrand as in equation (15).

Note that in the approximation of plane wave propagation discussed in the previous section, this PSF is much simpler since we do not have to take into account the factor ζ_M^{-2}, hence we only have

$$h^*(\boldsymbol{D}, \boldsymbol{V}; \theta) = n_e \frac{f_0}{4\pi} \rho^{-2} \sin^2 \theta \; P(\theta). \tag{38}$$

The fact that this PSF does not depend on ζ_V is consistent with the plane wave hypothesis.

4. Conclusion and perspectives

Based on physical analysis, we have found a new integral transformation, related to the formation of secondary images by Compton single-scattered photons in gamma-emission imaging. Moreover we have established that this transformation is *invertible*. This mathematical result gives a theoretical solution to the following ill-posed *inverse problem*: how to reconstruct the *volume* radioactive density of the object $f(\boldsymbol{V})$ from the intensity densities $g(\boldsymbol{D}, \theta)$ measured on a *planar* detector but at *various scattering angles* θ. Thus the relevance of this angle as a typical parameter is clearly displayed in the image reconstruction procedure. It plays the same role as the spatial rotation angle in a standard tomography procedure, where either the object or the detector is in motion. In the new imaging procedure, it is no longer necessary to move either the object or the detector. This result of course may pave the way to the conception of novel type of imaging devices, but their practical realization lies beyond the scope of this paper.

Finally these considerations could be extended to transmission imaging systems, where higher order Compton scatterings are to be taken into account and will be treated in future work.

Acknowledgments

We thank the referees for their suggestions leading to the improvement of the manuscript. We are also grateful to Professor H D Bui, Professor G Demoment and Professor A Bijaoui for discussions and encouragement throughout the course of this work.

References

[1] Barrett H H and Swindell W 1981 *Radiological Imaging* vol I and II (New York: Academic)
[2] Smith B D 1990 Cone beam tomography: recent advances and a tutorial review *Opt. Eng.* **29** 524–34
[3] Grangeat P 1990 Mathematical framework of cone beam 3D reconstruction via the first derivative of the Radon transform *Mathematical Methods in Tomography (Lecture Notes in Mathematics No 1497)* ed Herman *et al* (New York: Springer) pp 66–97
[4] Tam K C 1998 Computation of Radon data from cone beam data in cone beam imaging *J. Nondestruct. Eval.* **17** 1–15
[5] Tuy H K 1983 An inversion formula for cone-beam reconstruction *SIAM J. Appl. Math.* **43** 546–52
[6] Nguyen M K, Fay C, Eglin L and Truong T T 2001 Apparent image formation by Compton scattered photons in gamma-ray imaging *IEEE Signal Process. Lett.* **8** 248–51
[7] Radon J 1917 Über die Bestimmung von Funktionnen durch ihre Integralwerte längs gewisser Mannigfaltikeiten *Ber. Verh. Sachs. Akad. Wiss, Leipzig-Math.-Natur.Kl.* **69** 262–77
[8] Cree M J and Bones P J 1994 Towards direct reconstruction from a gamma camera based on Compton scattering *IEEE Trans. Med. Imaging* **13** 398–407
[9] Magnus W, Oberhettinger F and Soni R P 1966 *Formulas and Theorems for the Special Functions of Mathematical Physics* (New York: Springer)
[10] Davies B 2001 *Integral Transforms and Their Applications* (New York: Springer)
[11] Gelfand I M, Graev M I and Vilenkin N Ya 1966 *Generalized Functions* vol 1 and 5 (New York: Academic)
[12] Lavoine J 1963 *Transformation de Fourier des Pseudo-fonctions avec Tables de Nouvelles Transformées* (Paris: CNRS)
[13] Zaidi H 1999 Relevance of accurate Monte Carlo modeling in nuclear medical imaging *Med. Phys.* **26** 574–608